Chinese Chemical Letters 32 (2021) 2438–2442

Contents lists available at ScienceDirect

Chinese Chemical Letters

journal homepage: www.elsevier.com/locate/cclet

Communication

MOF-template derived hollow CeO_2/Co_3O_4 polyhedrons with efficient cathode catalytic capability in Li-O_2 batteries

Pengxiang Zhang[a,b,1], Jiajia Li[b,1], Juanjuan Feng[a], Yu Wang[b], Aili Xu[b], Tingting Chen[a], Lingwen Zhao[a], Feng Dang[b], Xihua Zhang[b,*], Hongchao Wang[a,*]

[a] School of Physics, State Key Laboratory of Crystal Materials, Shandong University, Ji'nan 250100, China
[b] Key Laboratory for Liquid-Solid Structural Evolution and Processing of Materials (Ministry of Education), Shandong University, Ji'nan 250061, China

ARTICLE INFO

Article history:
Received 30 December 2020
Received in revised form 2 February 2021
Accepted 2 February 2021
Available online 9 February 2021

Keywords:
Li-O_2 batteries
Co_3O_4
CeO_2
Hollow nanostructure
Cathode catalyst

ABSTRACT

Li-O_2 batteries (LOBs) have been perceived as the most potential clean energy system for fast-growing electric vehicles by reason of their environmentally friendlier, high energy density and high reversibility. However, there are still some issues limiting the practical application of LOBs, such as the large gap between the actual capacity level and the theoretical capacity, low rate performance as well as short cycle life. Herein, hollow CeO_2/Co_3O_4 polyhedrons have been synthesized by MOF template with a simple method. And it is was further served as a cathode catalyst in Li-O_2 batteries. By means of the synergistic effect of two different transition metal oxides, nano-sized hollow porous CeO_2/Co_3O_4 cathode obtained better capacity and cycle performance. As a result, excellent cyclability of exceeding 140 and 90 cycles are achieved at a fixed capacity of 600 and 1000 mAh/g, respectively. The successful application of this catalyst in LOBs offers a novel route in the aspect of the synthesis of other hollow porous composite oxides as catalysts for cathodes in LOBs systems by the MOF template method.

Although lithium-ion batteries have been extensively used in various mobile electronic equipments and started being applied in electric vehicles, the specific capacity is still relatively small compared to gasoline and cannot meet people's needs [1–5]. Lithium-oxygen battery batteries (LOBs) have been perceived as the most potential new energy system in the application of electric vehicles (EV) in years to come on account of their ultra-high energy density (10 times than lithium-ion batteries), environmental friendliness and high reversibility [6]. However, there still have many problems for current LOBs which affect the practical application of LOBs in industry, such as low actual specific capacity, high overpotential, and poor cycle performance [7,8].

For LOBs, the electrocatalytic performance is influenced by a variety of factors, while the decisive role is mainly the cathode catalyst. However, chemical reaction spontaneously occurs between conventional carbon materials (carbon nanotubes, graphene and so on) and the electrolyte and discharge product Li_2O_2, which leads to the formation of adverse coproducts [9,10]. Noble metals and their alloys have good catalytic properties, which can significantly reduce the overpotential of LOBs [11]. On the other hand, their reserves are very small and the price is too expensive to industrialize application. In this case, transition metal oxide which is low-cost and chemically stable has become a popular electrocatalytic material for LOBs [12–14]. Moreover, they have different kinds of microscopic morphologies and are easy to be controlled to form unique nanostructures. For example, Liu *et al.* directly grown flower-like δ-MnO_2 on graphene acted as the cathode catalyst for LOBs, which exhibits an exceptional specific capacity of 3660 mAh/g and cycles for more than 130 cycles [15]. Jian *et al.* synthesized CNT@RuO_2 compound with a core-shell structure and used as the cathode catalyst for LOBs, which effectively avoids the direct contact between CNT and the discharge product Li_2O_2, thereby reducing side reactions and improving the cycle capacity of the battery (more than 100 cycles at 500 mA/g and 500 mAh/g) [16]. Zhang *et al.* prepared MoO_3 nanosheets with different concentration of oxygen vacancies, which significantly decreases the overpotential (around 0.5 V) and obtains enhanced electrochemical property of LOBs (cycled over 60 cycles) [17].

As a stable dual-function catalyst, Co_3O_4 can play a highly effective catalytic role in both OER and ORR processes, and has been studied as a catalytic material for LOBs [18,19]. However, cathode has the low rate and cycle performance due to low

* Corresponding authors.
E-mail addresses: zhangxh@sdu.edu.cn (X. Zhang), wanghc@sdu.edu.cn (H. Wang).
[1] These authors contributed equally to this work.

https://doi.org/10.1016/j.cclet.2021.02.010
1001-8417/

catalytic efficiency and high overpotential, which are caused by poor conductivity of pure Co_3O_4 [20]. Therefore, Co_3O_4-based composite oxides have been employed to elevate the electrocatalytic properties of LOBs. Among them, CeO_2 has been regarded as the promising one due to its structural stability and high oxygen-ion conductivity [21,22]. In addition, with the change of external oxygen ion concentration, the cerium ions in CeO_2 are easily converted between the reduced state and the oxidized state, so it can be used as an oxygen pump to absorb and release oxygen during chemical reactions. Our previous work demonstrated that CeO_2 as the cathode catalyst in LOBs could work as oxygen pump to lower the overpotential during the ORR process [23,24]. The lattice matching between CeO_2 and the discharge product Li_2O_2 enables the CeO_2 as a grain promoter for the growth of Li_2O_2, which could enhance the conductivity of discharge products for the efficient decomposition Li_2O_2.

However, the electrochemical performances of LOBs not only depend on the catalytic capability but also the functional porous structure of cathode catalyst. Metal-organic frameworks (MOFs) are crystalline porous materials with periodic network structure formed by the self-assembly of transition metal ions and organic ligands [25,26]. It has the advantages of high porosity, low density, large specific surface area, regular pore, adjustable pore size and diversity of topological structure [27,28]. Therefore, this provides an attractive precursors template for constructing multifunctional composites. To date, a series of MOF-derived materials have been prepared successfully, which have shown great potential in oxygen reduction, water splitting, lithium ion batteries, *etc*. [29]. In the present work, we synthesize hollow CeO_2/Co_3O_4 polyhedrons as the cathode catalyst for LOBs. The CeO_2/Co_3O_4 polyhedrons are obtained from a MOF-derived synthesis process (ZIF-67). A hollow polyhedron with a mean grain size of around 200 nm is achieved, which can provide abundant exposed reactive sites, lead to a significant increase in the area of contact between the electrolyte and the catalyst, and promote the transmission of ions and electrons. In addition, the CeO_2/Co_3O_4 polyhedrons could exert the synergistic effect of the two compounds, activating the high oxygen ion conductivity of CeO_2 and the bifunctional catalytic performance of Co_3O_4, as well as the interplanar spacing matching Li_2O_2, for low overpotential and long cycle stability. As a result, CeO_2/Co_3O_4 polyhedrons cathode shows a specific capacity of 9443 mAh/g with the fixed current density of 100 mA/g and super rate properties of over 7126 and 5100 mAh/g at 200 and 500 mA/g. Moreover, long cycle stability of exceeding 140 and 90 cycles is exhibited with the fixed capacity of 600 and 1000 mAh/g.

The synthesis procedures and intermediate products of hollow CeO_2/Co_3O_4 polyhedrons are displayed in Scheme 1. Concisely, $Co(NO_3)_3{\cdot}6H_2O$ and 2-methylimidazole were co-precipitated in organic alcohol solvent to obtain ZIF-67. Afterwards, ZIF-67 was dispersed into the ethanol with Ce^{3+} dissolved. Through constant stirring, part of the Co^{3+} in the ZIF-67 structure was replaced by Ce^{3+} with a similar structure. After calcination, the color of the as-prepared product changed to black and the organic structure in the middle was ablated, implying the formation of hollow CeO_2/Co_3O_4 polyhedrons. Meanwhile, pure Co_3O_4 phase was also prepared as the control experiment using the same synthesis process without the exchange step.

SEM images show that the hollow CeO_2/Co_3O_4 polyhedrons obtain an average size of around 200 nm (Figs. 1a and b). Individual broken polyhedrons show that the inside is empty. This hollow polyhedron structure can offer a large specific surface area and homogeneous distribution of active sites, thereby increasing the area of contact, adsorbing faster of O_2 and wetting more comprehensively of electrolyte. Fig. 1c displays the microstructure of original intermediate ZIF-67. After ion exchanged by Ce^{3+}, the ZIF-67's dodecahedron shape becomes smooth, as depicted in Fig. 1d. Fig. S1 (Supporting information) showed that Ce and Co elements were uniformly distributed in ZIF-67 samples after Ce^{3+} ion exchange, indicating the successful introduction of Ce^{3+}. Fig. 1e displays the TEM images of hollow CeO_2/Co_3O_4 polyhedrons, it can be seen that the polyhedron structure is consisted of small nanosheets with a size of several nanometers. From the HRTEM image shown in Fig. 1f, the inter-planar spacing of 2.4 Å and 2.7 Å were corresponded to (311) plane of Co_3O_4 and (200) plane of CeO_2, were identified, respectively, indicating the existing of CeO_2 nanocrystals with a size of *ca.* 5 nm. In addition, similar hollow polyhedrons can be obtained without the addition of CeO_2 phase (Fig. S2 in Supporting information). The EDS-elemental mapping in Figs. 1g–i demonstrate that the elements of cobalt, cerium and oxygen were uniformly distributed within the CeO_2/Co_3O_4 polyhedrons, which further verifies the successful synthesis of the composite oxide and the unique core-shell structure.

XRD measurements are conducted to figure out the crystal structure of obtained samples. The XRD patterns of the hollow

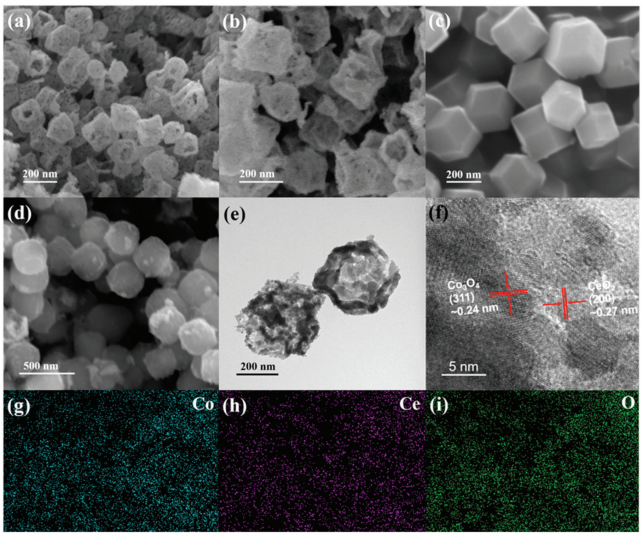

Fig. 1. (a, b) SEM images of fabricated hollow CeO_2/Co_3O_4 polyhedrons. (c) Images of synthesized ZIF-67. (d) Precursor of hollow CeO_2/Co_3O_4 polyhedrons obtained after Ce^{3+} replacement. (e, f) TEM images and HRTEM images of hollow CeO_2/Co_3O_4 polyhedrons. EDS-elemental mapping images of (g) cobalt, (h) cerium and (i) oxygen, respectively.

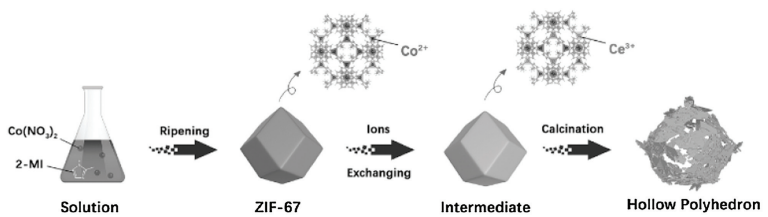

Scheme 1. Schematic illustration for the fabrication of hollow CeO_2/Co_3O_4 polyhedrons.

CeO_2/Co_3O_4 polyhedrons and MOF template (ZIF-67) are displayed in Fig. S3 (Supporting information). It was observed in Fig. S3a that all diffraction peaks strictly correspond to typical XRD pattern of synthesized ZIF-67, indicating that ZIF-67 was synthesized without any doubt and are consistent with the previous reports [30–33]. After ion exchanging, no peaks belonging to other phases were observed for the XRD pattern. However, several major peaks (002), (112), (222) move to the left slightly, which is attributed to the increase in lattice volume due to the doping of Ce^{3+} ions with larger radii (Fig. S3a). After calcination processes, diffraction peaks of Co_3O_4 and CeO_2 are exhibited without impurities, as shown in Fig. S3b. The diffraction reflections at 2θ of 36.9°, 59.4°, 65.2° correspond to (311), (511), (440) of Co_3O_4 (JCPDS No. 42-1467) and 28.6°, 47.5°, 56.2° correspond to (111), (220), (311) of CeO_2 (JCPDS No. 34-0394). The above results indicate the successfully formation of CeO_2/Co_3O_4 composites.

Afterwards, we further study the chemical states and the bonding configuration of the elements on the surface of the hollow CeO_2/Co_3O_4 polyhedrons through XPS measurements, as presented in Fig. 2. The peaks corresponding to Co 2p, Ce 3d and O 1s can be visibly observed in Fig. 2a, confirming that the hollow CeO_2/Co_3O_4 polyhedrons were successfully prepared. The peaks of two different valence of Co ions can be observed from Fig. 2b. The peaks at 777.8 and 793.0 eV belong to more active Co^{2+} while the other two peaks at 776.4 and 791.3 eV belong to Co^{3+} [34]. The peaks of Ce 3d displayed in Fig. 2c can be attributed to Ce^{4+} [22,35]. Three deconvoluted peaks at 529.7, 530.5 and 532.2 eV in O 1s high-resolution spectrum (Fig. 2d) correspond to the absorbed oxygen and lattice oxygen of Co/Ce-O bond on the surface of the sample. The XPS curve shows that Co_3O_4 has a higher concentration in the hollow CeO_2/Co_3O_4 polyhedron. According to the specific element composition, the atomic ratio of Ce/Co is calculated to be 0.14:1.

The nitrogen adsorption-desorption isotherm loop and pore size distribution curve of the hollow CeO_2/Co_3O_4 and Co_3O_4 polyhedrons are exhibited in Figs. S4a–d (Supporting information), which are obtained from the adsorption branch according to the Barrett-Joyner-Halenda (BJH) model. As a result, the surface area of obtained CeO_2/Co_3O_4 and Co_3O_4 polyhedrons is up to 58.885 and 52.417 m^2/g, respectively. The pore size distribution curve of both samples is almost similar owing to the same MOF-template. Porosity analysis performed in Figs. S4b and d shows the concentrated pore size is at about 20 nm, indicating that the samples have a mesoporous structure. This large specific area and mesopores of hollow CeO_2/Co_3O_4 polyhedrons will provide sufficient reaction sites for electrochemical reactions, which are conducive to the generation and growth of Li_2O_2 as discharge product. Furthermore, this structure also contributes to the diffusion and infiltration of the electrolyte better as well as the contact between electrolyte and electrode, ensures the rapid transmission of oxygen and Li^+, thereby realizing the enhancement of the capacity and cycle properties of LOBs.

The oxygen electrode of LOBs consists of KB and hollow CeO_2/Co_3O_4 polyhedron electrocatalyst. KB can serve as a conductor to offer enough conductivity and can be used as a matrix for the generation of discharge products. In a rechargeable LOB with 1 mol LiTFSI/TEGDME electrolyte, the CV differences between hollow CeO_2/Co_3O_4 polyhedrons and pure Co_3O_4 as electrodes are studied in 2.35–4.35 V voltage range, as Fig. 3a depicts. The hollow CeO_2/Co_3O_4 polyhedrons cathode shows both significantly higher cathodic ORR (2.72 V) and lower anodic OER (3.24 V) peak current with higher integral areas compared to that of Co_3O_4 cathode. In the first constant current discharge/charge curve below, the ORR onset potential matches the plateau voltage very well, which indicates that the hollow CeO_2/Co_3O_4 polyhedral electrode can achieve better catalytic activity and greater specific capacity. As shown in Fig. 3b, CeO_2/Co_3O_4 polyhedrons cathodes exhibit specific discharge capacities of 9443, 7126 and 5100 mAh/g at 2.35–4.34 V voltage window and 100, 200 and 500 mA/g current densities, indicating an exceptional rate performance and almost 100% Coulomb efficiency. During discharging, the average discharge voltages of all three different current densities are around 2.7 V. While during the charging process, the voltage platform gradually increases from only 4 V to 4.2 V with the increase of current density from 100 mA/g to 500 mA/g. The charge-discharge curves of the hollow CeO_2/Co_3O_4 polyhedrons and pure Co_3O_4 as cathodes are displayed in Fig. 3c at 200 mA/g current density. Higher capacitance and lower overpotential are obtained for the hollow CeO_2/Co_3O_4 polyhedrons cathode indicating the better catalytic activities compared to pure Co_3O_4. These reduced overpotentials and vaster capacity prove that the hollow CeO_2/Co_3O_4 polyhedron has enhanced performance as a LOB cathode catalyst.

The measurements of electrochemical impedance spectroscopy were carried out on LOBs at open circuit voltage in 10^5-0.1 Hz

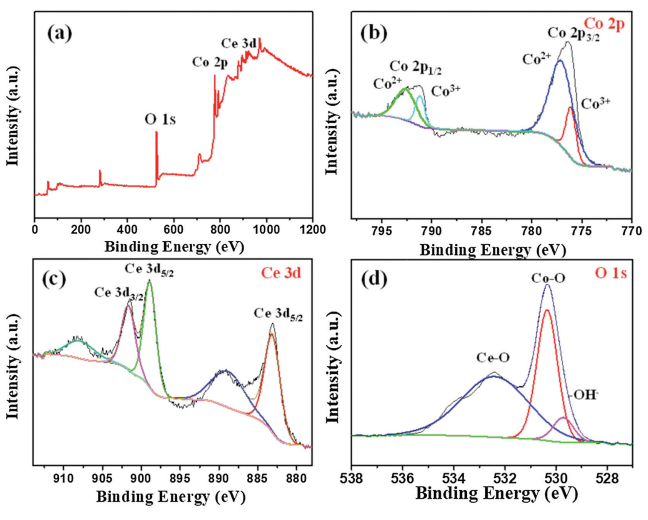

Fig. 2. (a) XPS survey spectrum for hollow CeO_2/Co_3O_4 polyhedrons. High-resolution (b) Co 2p, (c) Ce 3d and (d) O 1s XPS spectra for hollow CeO_2/Co_3O_4 polyhedrons.

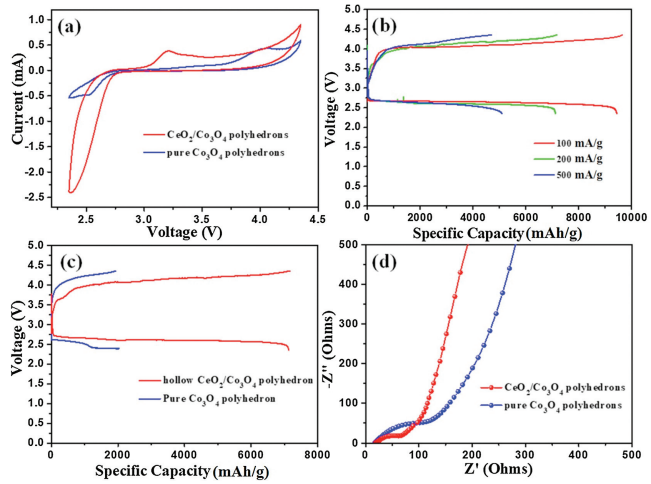

Fig. 3. (a) CV curves for hollow CeO_2/Co_3O_4 polyhedrons and pure Co_3O_4 cathodes. (b) Rate capabilities for hollow CeO_2/Co_3O_4 polyhedrons cathodes (at 100, 200 and 500 mA/g current density). (c) Charge-discharge profiles for hollow CeO_2/Co_3O_4 polyhedrons and pure Co_3O_4 at 200 mA/g. (d) EIS pattern of hollow CeO_2/Co_3O_4 polyhedrons and pure Co_3O_4 electrodes for LOBs.

frequency range to further illustrate the electrochemical properties of the hollow CeO_2/Co_3O_4 polyhedrons and pure Co_3O_4 electrodes, as shown in Fig. 3d. It can be calculated that CeO_2/Co_3O_4 polyhedrons have a lower impedance of 27.6 Ω than pure Co_3O_4 (52.8 Ω) on the grounds of the semicircle in the mid-frequency region, supporting that CeO_2/Co_3O_4 polyhedrons have better conductivity. The apparent difference can be ascribed to the existence of CeO_2, the synergy of the bimetallic oxide and the hollow structure which contribute to the adsorption and decomposition of discharge product. The improved dynamics in ORR/OER can effectively increase the energy output, charging characteristics and round-trip efficiency of the LOBs.

Excellent cycle performance of hollow CeO_2/Co_3O_4 polyhedrons cathodes for LOBs is achieved as expected, which cycles more than 140 and 90 cycles at 100 mA/g current density with 600 and 1000 mAh/g fixed capacity respectively, as shown in Fig. 4. Figs. 4a and b present the curves of discharge/charge and terminal voltages for hollow CeO_2/Co_3O_4 polyhedrons cathodes during the cycles with specific capacity of 600 mAh/g. For comparison, the cycle performance of the samples sintered at 300 and 500 °C were also tested at the current density of 100 mA/g with a fixed capacity of 1000 mAh/g and shown in Fig. S5 (Supporting information). The sample sintered at 400 °C exhibited best cycle performance. The discharging voltage starts from 2.7 V at the first cycle and decreases to 2.5 V after 100 cycles, then to below 2.0 V after 140 cycles. At the same time, the charging voltage platform increases from about 4.1 V to 4.4 V. As long as the specific capacity is up to 1000 mAh/g (Figs. 4c and d), the discharging voltage decreases to below 2.0 V after 95 cycles and the charging voltage platform increases to 4.5 V. The increase in overpotential is also clearly seen from the terminal voltage curves, which may be caused by the degradation of the CeO_2/Co_3O_4 electrode during the cycles. The degradation of the CeO_2/Co_3O_4 electrode can be attributed the surface and structure evolution of spinel Co_3O_4 [12,36]. Dang *et al.* revealed that the surface condition and inside structure of spinel crystal structure would change to unstable during cycling in LOBs [12,36]. Further, the side reaction was also one of the main reasons for the degradation of CeO_2/Co_3O_4 electrode. The excellent performance for hollow CeO_2/Co_3O_4 polyhedrons samples is mainly attributed to the introduction of CeO_2. Hou *et al.* reported that the valence of Ce ions and oxygen vacancy concentration in CeO_2 would change constantly due to the ORR/OER reaction process [4]. Furthermore, the formation of Li_2O_2 was identified to be significantly accelerated due to lattice matching between CeO_2 and Li_2O_2 [10,24]. It can be concluded that the CeO_2 can accelerate the initial nucleation of Li_2O_2 and act as oxygen buffer for efficient decomposition of discharge products. Further, the cycle performance of pure Co_3O_4 polyhedron was also showed in Fig. S6 (Supporting information). It can be seen that the cycle performance of Co_3O_4 was poor compared to that of CeO_2/Co_3O_4 electrode.

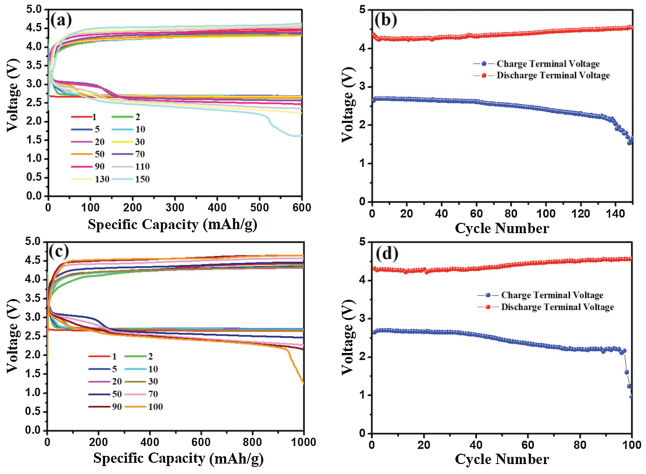

Fig. 4. (a) The cycle performance and (b) discharge/charge terminal voltages for hollow CeO_2/Co_3O_4 polyhedrons cathode at 100 mA/g current density and 600 mAh/g specific capacity limit. (c) The cycle performance and (d) terminal voltages of hollow CeO_2/Co_3O_4 polyhedrons cathode at a current density of 100 mA/g and 1000 mAh/g specific capacity limit.

The evolution of discharge product on the cathodes was examined in the process of discharge/charge by means of the *ex-situ* SEM images and XRD patterns, as shown in Fig. S7 (Supporting information). Fig. S7a shows the SEM images of fresh CeO_2/Co_3O_4 polyhedrons. When discharged to 1000 mAh/g, a layer of discharge product is generated on the surface of CeO_2/Co_3O_4 polyhedrons as shown in Fig. S7b. After recharged with the same capacity, the layer of discharge product on CeO_2/Co_3O_4 polyhedrons is completely decomposed, shown in Fig. S7c, indicating the good reversibility. The variation of the cathode material in the first process of discharging and charging was examined by XRD in order to make a thorough inquiry in the generation and decomposition of discharge products in Fig. S7d. The XRD pattern of CeO_2/Co_3O_4 polyhedrons cathode for LOBs shows peaks corresponding to Li_2O_2 phase (JCPDS No. 73-1640) after first discharging. What attracts attention is that the peak at 32.8° corresponding to (001) plane of Li_2O_2 is higher than the other peaks, and it is caused by the matching interplanar spacing between the (200) plane of CeO_2 (2.72 Å) and the (100) plane of Li_2O_2 (2.74 Å), attributing the oriented growth of Li_2O_2 on the surface of cathode catalyst. After recharged to the same capacity, all the peaks of Li_2O_2 disappear, indicating the completely decomposed of discharge product and the excellent reversible performance of the CeO_2/Co_3O_4 polyhedrons cathode. Furthermore, the changes of EIS data during the cycles is also tracked, as presented in Fig. S7e. The pristine cathode reveals a small charge transfer resistance (R_{ct}) of 27.6 Ω in the mid-frequency domain, which means that the interface between the electrolyte and the electrode has good conductivity. After the first discharge, the R_{ct} for CeO_2/Co_3O_4 polyhedrons cathodes is 138.64 Ω, which far exceeds than original voltage. This may be attributed to the generation of discharge product Li_2O_2 on the electrode surface. While, after the first charge, the R_{ct} reduces to 65.25 Ω as the discharge product Li_2O_2 which produced in the process of discharge almost entirely decomposed on account of the catalysis of CeO_2/Co_3O_4 polyhedrons. Moreover, after 20^{th}, 50^{th} and 100^{th} discharged, the charge transfer resistances slightly increase to 76.32, 98.85 and 125.20 Ω, respectively. These results demonstrate excellent cycle performance and favorable reversibility have been found for the discharge products Li_2O_2 in the LOBs.

In summary, hollow CeO_2/Co_3O_4 polyhedrons have been fabricated from MOF-template (ZIF-67) and successfully used as the efficient cathode catalyst in LOBs. This hollow polyhedron structure with a mean size of roughly 200 nm combined with the mesopores of *ca.* 20 nm effectively increases the area of contact between electrolyte and the cathode catalytic material, then shortens the length of the diffusion path between Li-ion and oxygen, increases the storage capacity of the discharge product Li_2O_2. Therefore, LOBs using CeO_2/Co_3O_4 polyhedrons cathode exhibit 9443 mAh/g specific capacity at the 100 mA/g current density of and obtain super rate properties of more than 7126 and 5100 mAh/g at 200 and 500 mA/g. Moreover, at the 600 and 1000 mAh/g fixed capacity, CeO_2/Co_3O_4 polyhedrons cathode could be galvanostatically cycled exceeding 140 and 90 cycles. Through the combination of the two transition metal oxides and the promotion of the hollow structure, CeO_2/Co_3O_4 polyhedrons cathode exhibit excellent electrochemical performance in LOB systems, which

offers a novel route for fabrication and application of other transition metal oxides in LOBs.

Declaration of competing interest

The authors report no declarations of interest.

Acknowledgments

The work is financially supported by National Key R&D Program of China (No. 2017YFE0195200), the Natural Science Fund of China (Nos. 51871134, 51672159), the Science Fund of Shandong Province (No. ZR2019MEM007).

Appendix A. Supplementary data

Supplementary material related to this article can be found, in the online version, at doi:https://doi.org/10.1016/j.cclet.2021.02.010.

References

[1] D. Larcher, J.M. Tarascon, Nat. Chem. 7 (2015) 19–29.
[2] B. Zakeri, S. Syri, Renew. Sustain. Energy Rev. 42 (2015) 569–596.
[3] O.Z. Sharaf, M.F. Orhan, Renew. Sustain. Energy Rev. 32 (2014) 810–853.
[4] C. Hou, Y. Hou, Y. Fan, et al., J. Mater. Chem. A 6 (2018) 6967–6976.
[5] C. Hou, G. Fan, X. Xie, et al., J. Alloys Compd. 855 (2021) 157499.
[6] Z. Peng, S.A. Freunberger, Y. Chen, P.G. Bruce, Science 337 (2012) 563–566.
[7] N. Feng, P. He, H. Zhou, Adv. Energy Mater. 6 (2016) 1502303.
[8] C. Dang, Y. Wang, B. He, et al., J. Mater. Chem. A 8 (2020) 259–267.
[9] M.M. Ottakam Thotiyl, S.A. Freunberger, Z. Peng, P.G. Bruce, J. Am. Chem. Soc. 135 (2013) 494–500.
[10] Y. Hou, J. Wang, J. Liu, et al., Adv. Energy Mater. 9 (2019) 1901751.
[11] F.S. Gittleson, W.H. Ryu, M. Schwab, X. Tong, A.D. Taylor, Chem. Commun. 52 (2016) 6605–6608.
[12] B. He, J. Wang, J. Liu, et al., Adv. Energy Mater. 10 (2020) 1904262.
[13] X. Mu, Q. Wen, G. Ou, et al., Nano Energy 51 (2018) 83–90.
[14] M. Yuan, R. Wang, W. Fu, et al., ACS Appl. Mater. Interfaces 11 (2019) 11403–11413.
[15] S. Liu, Y. Zhu, J. Xie, et al., Adv. Energy Mater. 4 (2014) 1301960.
[16] Z. Jian, P. Liu, F. Li, et al., Angew. Chem. Int. Ed. 53 (2014) 442–446.
[17] S. Zhang, G. Wang, J. Jin, et al., Nano Energy 36 (2017) 186–196.
[18] S.H. Peng, T.H. Chen, C.H. Lee, H.C. Lu, S.J. Lue, J. Power Sources 471 (2020) 228373.
[19] W.H. Ryu, T.H. Yoon, S.H. Song, et al., Nano Lett. 13 (2013) 4190–4197.
[20] Y.M. Chen, L. Yu, X.W. Lou, Angew. Chem. Int. Ed. 55 (2016) 5990–5993.
[21] M.C. Sung, G.H. Lee, D.W. Kim, Nanoscale 10 (2018) 21292–21297.
[22] Y. Jiang, J. Cheng, L. Zou, et al., Electrochim. Acta 210 (2016) 712–719.
[23] Y. Hou, J. Wang, C. Hou, et al., J. Mater. Chem. A 7 (2019) 6552–6561.
[24] Y. Wang, J. Wang, Z. Mohamed, et al., Appl. Mater. Today 19 (2020) 100603.
[25] L. Lu, B. Wu, W. Shi, P. Cheng, Inorg. Chem. Front. 6 (2019) 3456–3467.
[26] Q. Lan, Z.M. Zhang, C. Qin, et al., Chem. Eur. J. 22 (2016) 15513–15520.
[27] C. Chen, A. Wu, H. Yan, et al., Chem. Sci. 9 (2018) 4746–4755.
[28] R.J. Wu, M. Liu, Y.-W. Peng, et al., Chin. Chem. Lett. 30 (2019) 989–994.
[29] M. Liu, L.Z. Qiao, B.-B. Dong, et al., Appl. Catal. B: Environ. 273 (2020) 119066.
[30] Y. Wang, X. Di, X. Wu, X. Li, J. Alloys Compd. 846 (2020) 156215.
[31] V. Shrivastav, S. Sundriyal, A. Kaur, et al., J. Alloys Compd. 843 (2020) 155992.
[32] Y.H. Zou, H.N. Wang, H.X. Sun, et al., Mater. Chem. Phys. 255 (2020) 123497.
[33] H. Guo, T. Fan, W. Yao, et al., Microchem. J. 158 (2020) 105262.
[34] D. Yu, Y. Wang, L. Zhang, et al., Nano Energy 10 (2014) 153–162.
[35] C. Cao, J. Xie, S. Zhang, et al., J. Mater. Chem. A 5 (2017) 6747–6755.
[36] Q. Huang, B. He, W. Zhang, et al., ACS Appl. Mater. Interfaces 12 (2020) 30268–30279.